ELSEVIER

International Journal of Mass Spectrometry 212 (2001) 229–247

www.elsevier.com/locate/ijms

Internal energy distribution in charge inversion mass spectrometry using alkali metal targets

Shigeo Hayakawa*

College of Integrated Arts and Sciences, Osaka Prefecture University, Gakuencho 1-1, Sakai, Osaka, 599-8531, Japan

Received 26 April 2001; accepted 9 August 2001

Abstract

A charge inversion mass spectrometer (PMS/NMS) by using alkali metal targets has been developed which produces clearer differentiation of hydrocarbon isomers than collision induced dissociation (CID). In PMS/NMS, mass-selected positive ions are made to collide with an alkali metal target, and the resulting negative ions formed upon two-electron transfer are mass analyzed. On the basis of the observed target-density dependence of product ion intensity and thermochemical considerations, we propose that the process of dissociative negative ion formation in PMS/NMS is by way of near-resonant neutralization, followed by spontaneous dissociation of the neutrals and then endothermic negative ion formation. CID spectra and PMS/NMS spectra have been measured for two types of so-called thermometer molecules, namely partially deuterated methanol and $W(CO)_6$. The differences between the CID spectra and the PMS/NMS spectra of partially deuterated methanol demonstrate that the major process in PMS/NMS involves dissociation of the excited neutral species. The internal energy deposition of the charge inversion measured for $W(CO)_n^+$ ($n = 4–6$) ions indicates that dissociation occurs in the energy-selected neutrals formed by way of near-resonant neutralization. The relative peak intensities in the PMS/NMS spectra for some hydrocarbons depend strongly on the alkali metal target used, indicating the importance of internal energy in the dissociation of the excited neutral intermediates. These results demonstrate the utility of PMS/NMS as a technique for the investigation of the dissociation of energy-selected neutral intermediates and for isomeric differentiation. (Int J Mass Spectrom 212 (2001) 229–247) © 2001 Elsevier Science B.V.

Keywords:

1. Introduction

Tandem mass spectrometry (MS/MS) [1,2] and metastable ions [3] provide a range of information about discrimination of isomers, characterization of ion structure, and the dissociation mechanism of ions. Although metastable ions dissociate spontaneously without the benefit of an activation reaction, MS/MS usually requires the use of collisional activation in order for the precursor ions to dissociate effectively. A variety of methods for excitation of precursor ions have been developed, such as high-energy collision induced dissociation (CID) [1,2,4–7], low-energy CID [1,2,8–10], surface induced dissociation (SID) [2,11–15], and electron transfer [16]. The dissociation mechanism of the excited ions depends on the internal energy of the ions [17], and the internal energy

* Corresponding author. E-mail: hayakawa@ms.cias.osakafu.u.ac.jp

Dedicated to R. Graham Cooks on the occasion of his sixtieth birthday.

PII S1367-3806(01)00518-8

distribution of excited ions in MS/MS has been measured by using thermometer molecules such as metal carbonyls and alkyl silanes. These measurements were mainly reported by Cooks and co-workers using CID [17–21], SID [14,22–24], and electron transfer in doubly charged ions [25–28]. This type of information about internal energy distribution is valuable not only for ions but also for neutrals because the dissociation of excited neutrals is one of the most important types of chemical reaction.

Although mass spectrometry is well suited to the study of the dissociation of various stable and unstable ions, the investigation of neutral species using mass spectrometry has been difficult due to their lack of electronic charge. To investigate the dissociation of neutral species, high-energy neutral detection methods were developed by Porter and co-workers [29–32], although these methods could not identify the mass of fragment neutrals. Los and co-workers reported [33–36] the dissociation mechanism for simple molecules using a coincident technique measuring position and time differences. However, loss of hydrogen atoms from polyatomic molecules, such as hydrocarbons, was not studied using the coincident method because this method could not analyze fragments with mass ratios larger than 6.2 [37,38]. Peterson and co-workers reported [39–44] the dissociation of neutrals formed by means of electron transfer from ions not having stable neutral counterparts. Neutralization reionization mass spectrometry (NRMS) has also been developed as a method for generation and structural characterization of neutral species [45–49]. Recently, the chemical reactivity of neutral species in the gas phase was studied by Turecek and co-workers [50–52] using advanced NRMS methods such as photoexcitation, photoionization and long-distance NR, and the results of neutral and ion decomposition difference (NIDD) studies were reported by Schwarz and co-workers [53,54].

The alternative technique of charge inversion mass spectrometry (PMS/NMS) using alkali metal targets has been developed independently by the present author and co-workers [55–67]. Charge inversion reactions to form negative ions have been reported for the precursor positive ions obtained by electron impact on hydrogen [55,56], hydrocarbons [57–63], tungsten hexacarbonyl [64], partially deuterated methanol [65,66], and dichlorobenzene [67]. On the basis of the observed target-density dependence of product negative ion intensity and the internal energy distribution determined in these works, it was proposed that the process of dissociative negative ion formation in charge inversion mass spectrometry occurs by way of near-resonant neutralization followed by spontaneous dissociation of the neutrals and then endothermic negative ion formation, and that the dissociation of neutral intermediates can be investigated by this method. In the present work, along with providing some new data, we review these previous studies, with particular emphasis on the internal energy distribution in charge inversion mass spectrometry using alkali metal targets. The differences in the internal energy distribution between PMS/NMS and the dissociation of positive ions by CID, SID, and electron transfer are also discussed. These results demonstrate the utility of PMS/NMS as a technique for isomeric differentiation and for the investigation of the dissociation of energy selected neutral intermediates.

2. Experiment

Mass-selected positive ions are made to collide with alkali metal targets, and the resulting negative ions formed upon two-electron transfer are mass analyzed in the charge inversion mass spectrometer which is a MS/MS instrument, as shown schematically in Fig. 1. Positive precursor ions are formed by electron impact ionization and are accelerated to a kinetic energy of 3 keV. The precursor ions are mass selected by a Hitachi M80B double focusing mass spectrometer (MS-I). The central radius of the electric sectors is 216 mm, and the magnetic field has a 200 mm ion orbital radius. The mass-selected precursor ions enter a 3 cm long target chamber, which is located between the two analyzers. The alkali metal target is introduced into the target chamber as a vapor from a reservoir through a ball valve. The target chamber, the ball valve and the reservoir are ther-

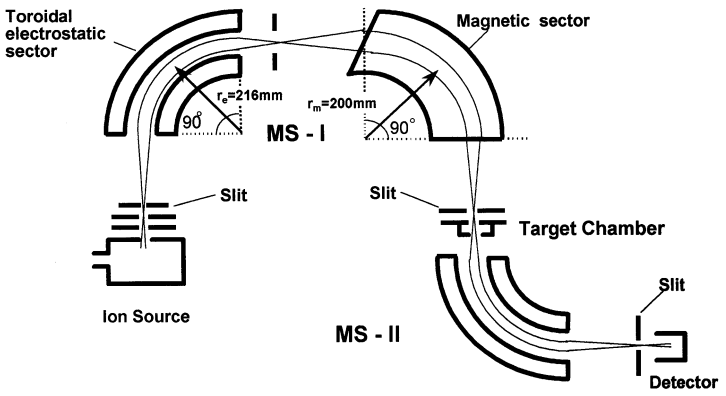

Fig. 1. Schematic diagram of the charge inversion MS/MS instrument. Positive precursor ions are mass selected by MS-I. Alkali metal targets were introduced into the target chamber. For collision induced dissociation (CID) spectra, the positive ions were measured by MS-II. For charge inversion spectra, the negative ions were mass analyzed by MS-II, after the polarities of MS-II and the detector were changed.

mally controlled in order to control the alkali metal density in the target chamber. Neutralization, dissociation, and anionization take place in the target chamber filled with alkali metal vapor. The negative ions are mass analyzed by a cylindrical electrostatic analyzer (ESA) with a 216 mm central radius (MS-II). The mass-analyzed negative ions are detected by a 10 kV postacceleration secondary electron multiplier. When the supply of alkali metal vapor from the reservoir is stopped by closing the ball valve, all of the negative ion peaks in the charge inversion spectra disappear, indicating that the negative ions are generated by the collision of the positive ions with alkali metal targets.

CID spectra were measured by mass analyzing the positive ions exiting the target chamber. By changing the polarity of MS-II and the multiplier, the positive ions were mass analyzed by MS-II and the mass-analyzed secondary ions were detected by the multiplier. CID spectra were measured usually with alkali metal target, but sometimes with a rare gas target by changing the gas inlet system of the target chamber.

Acetylene (99.6%, Takachiho, Japan) and tungsten hexacarbonyl (99%, Aldrich, USA), $W(CO)_6$, were used as received. Two types of partially deuterated methanol, namely CH_3OD and CD_3OH (Merck), were also used as received. The level of deuterium content of both molecules was >99%.

3. Results and discussion

3.1. Reaction processes in charge inversion mass spectrometry using alkali metal targets

In charge inversion mass spectrometry using alkali metal targets, dissociative negative ions formed from positive ions by transfer of two electrons are overwhelmingly more abundant than nondissociative negative ions [55–67]. It is possible that the formation of the negative product ions produced by transfer of two electrons in the charge inversion mass spectrometer may involve either double electron transfer in one collision or successive single electron transfers in two collisions. The determination of which of these processes dominates in charge inversion mass spectrometry is essential because the dissociation mechanism depends strongly on the electron transfer process. The reaction process for double electron transfer in a single

$$AB^+ + T \rightarrow AB^{-}* + T^{2+} \quad (1)$$

$$AB^{-}* \rightarrow A + B \quad (2)$$

The reaction process for successive single electron transfers in two collisions is shown in

$$AB^+ + T \rightarrow AB* + T^+ \quad (3)$$

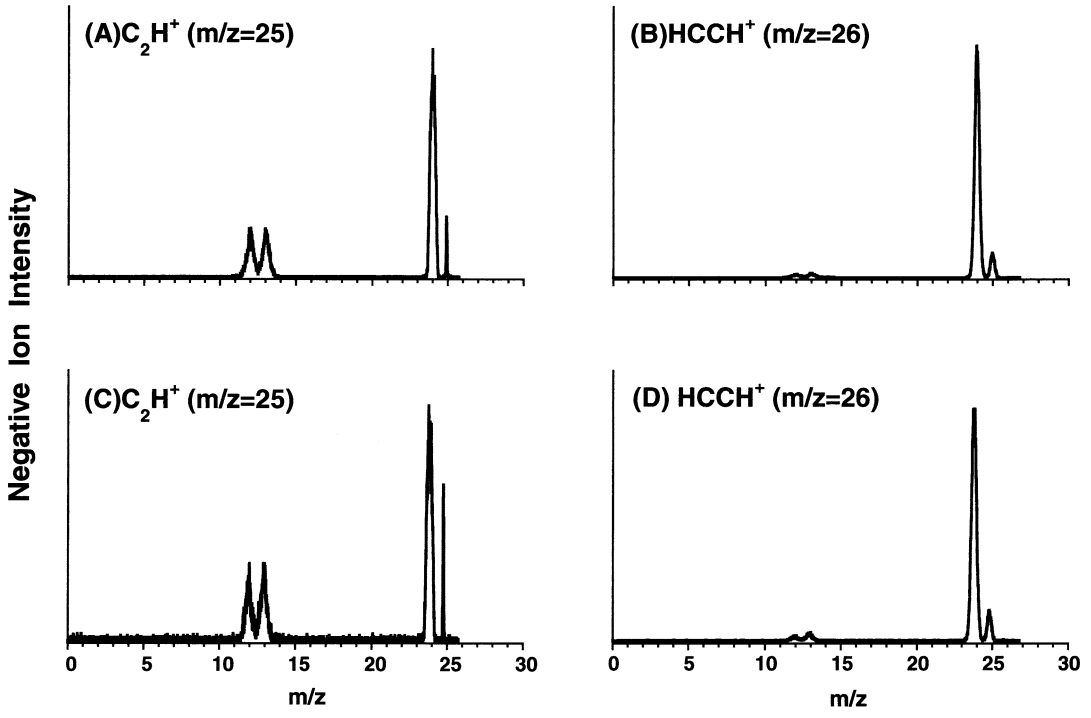

Fig. 2. PMS/NMS spectra of (A and C)C_2H^+ ions and (B and D) $C_2H_2^+$ ions. The experimental conditions for (A) and (B) are identical except for the precursor ions, and so are those for (C) and (D). The target density for (A) and (B) is about 2.5 times higher than that for (C) and (D). The nondissociative C_2H^- ion formation shows a different dependence on the target density than the dissociative C_2^- ion formation.

$$AB^* \rightarrow A + B \quad (4)$$

$$B + T \rightarrow B^- + T^+ \quad (5)$$

where the dissociation takes place after neutralization, as discussed in the following.

3.1.1. Target density dependence of negative ions formed from positive ions by meand of two electron transfer

The PMS/NMS spectra of C_2H^+ ions ($m/z = 25$) and $C_2H_2^+$ ions ($m/z = 26$) obtained by electron impact on acetylene are shown in Fig. 2(A) and (B), respectively. As the spectra of C_2H^+ ions and $C_2H_2^+$ ions measured alternately were averaged several times, the experimental conditions of Fig. 2(A) and (B) were identical except for the mass number of the precursor ions. Although the spectra of C_2H^+ ions ($m/z = 25$) and of $C_2H_2^+$ ions ($m/z = 26$) shown in Fig.2(C) and (D), respectively, were also measured under identical conditions, the target density used to obtain the spectra in Fig. 2(A) and (B) was 2.5 times larger than that of Fig. 2(C) and (D). In Fig. 2(A) and (C), nondissociative C_2H^- ions are observed at $m/z = 25$ as a sharp peak. As seen from the comparison of Fig. 2(A) and (C), the relative intensity of nondissociative C_2H^- ions ($m/z = 25$) to that of dissociative C_2^- ions became much smaller as the target density increased. The relative intensity of dissociative C_2^- ions ($m/z = 24$) ions and C_2H^- ions ($m/z = 25$) ions formed from $C_2H_2^+$ ions was independent of target density, as seen from the comparison of Fig. 2(B) and (D). The dependence of target density for these dissociative ions observed in Fig. 2(B) and (D) are comparable to that for the dissociative C_2^- ions observed in Fig. 2(A) and (C). This difference in dependence on the target density of dissociative ions compared with nondissociative ions indicates that the collision process responsible for dissociative ions

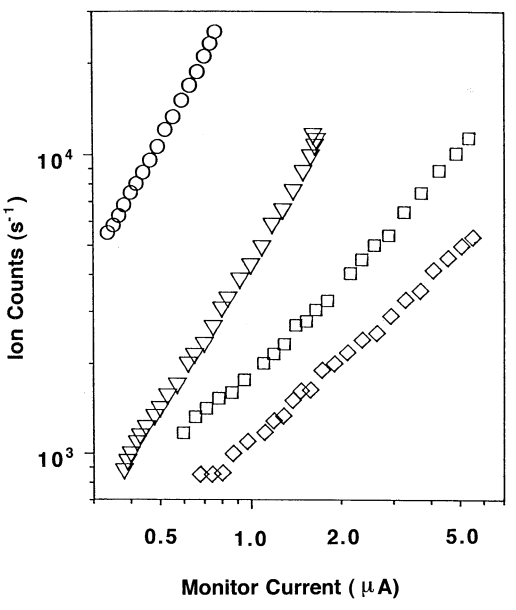

Fig. 3. Target density dependence of product negative ion intensities measured by the single-focusing charge inversion mass spectrometer. The target was Cs. He^- ions from He^+ ions (open circle); dissociative C_2^- ions from $C_2H_2^+$ ions (inverted open triangle); nondissociative C_2^- ions from C_2^+ ions (open square); nondissociative C_2H^- ions from C_2H^+ ions (open diamond). Although He^- ions and dissociative C_2^- ions display a square dependence on the target density, nondissociative C_2^- and C_2H^- ions show a linear dependence.

observed in PMS/NMS spectra is likely to be different from that for the nondissociative ions.

By using the single-focusing charge inversion mass spectrometer at Osaka Prefecture University, we have measured the target density dependence of the product negative ions by monitoring the target density using surface ionization of the alkali metal target [57–59]. The negative ion intensities versus the monitor currents, which was proportional to the target density of the alkali metal vapor in target chamber, are plotted in Fig. 3. The monitor comprises a stainless-steel tube collector and 1 mm width heated tungsten ribbon filament, and measures the surface-ionized current of the alkali metal, which flowed through the hole drilled in the target chamber. The monitor current is proportional to the target density calculated from the temperature of the alkali metal reservoir [59].

He^- ions obtained from He^+ ions are plotted in Fig. 3 for comparison. He^- ion formation was reported as two collision processes by the reaction [68]

$$He^+ (1s) + Cs \rightarrow He^* (1s2s) + Cs^+ \quad (6)$$

$$He^* (1s2s) + Cs \rightarrow He^{-*} (1s2s2p) + Cs^+ \quad (7)$$

The square dependence of He^- ion formation on the target density shows that this measurement for density dependence is reliable. As seen in Fig. 3, dissociative C_2^- ion formation from $C_2H_2^+$ ions displays a square dependence, in the same manner as He^- ion formation. In contrast to dissociative negative ion formation, nondissociative C_2^- and C_2H^- ion formation displays a linear dependence on the target density.

As precursor positive ions were not selected by the single-focusing charge inversion mass spectrometer at Osaka prefecture university, peaks associated with negative ions from different positive precursor ions were observed in a charge inversion spectrum [55–59]. Dissociative C_2^- ion formation from C_2H^+ and C_2H^- ion formation from $C_2H_2^+$ ions showed the same dependence on the target density as dissociative C_2^- ion formation from $C_2H_2^+$ ions at various target density conditions. The different target density dependence of nondissociative negative ion formation compared with dissociative negative ion formation obtained using the single-focusing charge inversion mass spectrometer is in accordance with those of the peaks observed in the PMS/NMS spectra shown in Fig. 2(A) and (C). From these measurements, it was confirmed that nondissociative C_2^- and C_2H^- ion are formed by double electron transfer in a single collision [reaction (1)], whereas dissociative C_2^- and C_2H^- ions are formed by the successive single-electron transfer in two collisions [reactions (3) and (4)].

3.1.2. Thermochemical consideration of the double electron transfer in a single collision and successive single electron transfer in two collisions

The endothermicity (ΔE) for the double electron transfer in a single collision for a projectile (AB) and a target (T) is given by

Table 1
Ionization energies (IEs) and electron affinities (EAs) of relevant species in electron volts; IEs for alkali metal targets are cited from [69]

Species	First IE	Second IE	EA[a]
Cs	3.893	25.08	
K	4.339	31.81	
Na	5.138	47.29	
C_2	12.11[b]		3.269
C_2H	11.96[c]		2.969

[a]See [70].
[b]See [71].
[c]See [72]

$$\Delta E = \mathrm{IE}(T) + \mathrm{IE}(T^+) - \mathrm{IE}(AB) - \mathrm{EA}(AB) \quad (8)$$

where IE and EA are ionization energy and electron affinity, respectively. The ionization energies and electron affinities relevant to this discussion are shown in Table 1 [69–72]. Although alkali metals have small ionization energies, IE(T), alkali metal cations have large ionization energies, IE(T^+), as shown in Table 1. The experimental [73–75] and theoretical [76,77] treatment for double electron transfer in one collision indicates the existence of a reaction window for the reactions. Langford and Harris reported that the reaction window for the CH_3Br target is between endothermicities of about 8 and 22 eV using the S^+, OH^+, and F^+ ions as the projectile [74]. Griffiths et al. also reported that when the projectile is either 6 keV OH^+ or F^+ ions and the collision gas consists of fluorinated benzene molecules, then the cross section for the reaction maximizes when the reaction endoergicity has a value between 10 and 14 eV [75].

The endothermicities of double electron transfer to form C_2^- ions and C_2H^- ions are shown in Table 2. In double electron transfer forming nondissociative C_2^- and C_2H^- ions using alkali metal targets, the endothermicity for the Cs target only is in this reaction window, that for K is at the upper limit, and that for Na is out of it, as seen from the endothermicities in Table 2. This prediction for the reaction window is in accordance with our experimental results, in which the double electron transfer processes were observed only for the Cs target and not for K and Na targets [57,60]. For H^- ion formation from H^+ ions, cross-section data have been compiled by Tawara and Russek [78] and Nakai et al. [79]. Most of the absolute cross sections for double electron transfer in one collision are in the order of 10^{-18}–10^{-17} cm^2 in the kiloelectron volt energy range. The absolute cross section measured for C_2^- and C_2H^- ion formation by way of double electron transfer in one collision with a Cs target is in the order of 10^{-18}–10^{-17} cm^2 [57,60].

Table 2
Endothermicities for double electron transfer in single collisions in eV; these values were calculated from the IEs and EA in Table 1 using Eq. (8)

	Cs	K	Na
C_2	13.59	20.77	37.05
C_2H	14.04	21.22	37.50

If dissociative negative ions are formed from double electron transfer in a single collision [reactions (1) and (2)], then the bond energy for the dissociation must be added to the endothermicities of the double electron transfer reaction. As a result of the large endothermicity, the cross sections of double electron transfer accompanied with the bond dissociation are estimated to be small. A decrease in electron affinity results in a larger endothermicity, as seen in Eq. (8), and the reaction cross section is expected to decrease due to the larger endothermicity. Although $W(CO)_4$ and vinylidene have positive electron affinities, nondissociative $W(CO)_4^-$ and vinylidene anion were not observed in the PMS/NMS spectra using alkali metal targets [63,64]. For acetylene and methanol, both which have negative electron affinities, it is unlikely that the dissociative negative ions are formed from the dissociation of unstable $C_2H_2^-$* and CH_3OH^-* ions, respectively, formed from double electron transfer.

The endothermicity (ΔE) for the neutralization [reaction (3)] for a projectile (AB) and a target (T) in successive single electron transfers in two collisions is given by

$$\Delta E = \mathrm{IE}(T) - \mathrm{IE}(AB) + \mathrm{EE}(AB) \quad (9)$$

where IE, EA, and EE are ionization energy, electron affinity, and excitation energy (the internal energy of AB), respectively. For electron transfer in the kiloeelectron volt collision energy region, near-resonant reaction ($\Delta E \sim 0$) affords a larger cross section than exothermic and endothermic reactions [80,81]. The cross-section data of charge transfer for hydrogen ions in collision with alkali metal targets were compiled by Morgan et al. [82] and Tabata et al. [83]. The neutralization cross section for H^+ ions using alkali metal target were in the order of 10^{-15}–10^{-14} cm^2 in the kiloelectron volt energy range. Resonant and near-resonant neutralization cross sections for organic molecules were also reported to be of the same order of magnitude [84]. The cross-section data compiled for alkali metal targets indicates that the neutralization reaction with alkali metal targets has preference over the double electron transfer process. If near-resonant neutralization occurs with alkali metal targets, the neutral species formed by electron transfer may be excited at the energy EE(AB) = IE(AB) − IE(T) because the ionization energies of hydrocarbons are usually larger than those of alkali metals.

The endothermicity (ΔE) for negative ion formation [reaction (5)] for a projectile (B) and a target (T) in successive single electron transfers in two collisions is given by

$$\Delta E = \text{IE}\,(T) - \text{EA}\,(B) \tag{10}$$

Although the ionization energies of alkali metals are the smallest among atoms, electron affinities of hydrocarbon molecules and radicals are usually smaller than the ionization energies of alkali metals [70]. The energy of the lowest electronic excitation level of alkali metal cations is more than 10 eV [69] and the excitation of negative ions results in spontaneous electron detachment. Therefore both the product ions are expected to be in their respective electronic ground states, and most of the endothermicities of negative ion formation with alkali metals are estimated to be a few eV. This small endothermicity associated with forming of ground state products is likely to afford larger cross sections than those of the more highly endothermic reactions accompanied with dissociation of product negative ions.

3.2. Dissociation mechanism of neutral intermediates in PMS/NMS

3.2.1. Comparison between PMS/NMS and neutral detection methods

Because product negative ions were analyzed only by the energy selector of the electric sector field in the PMS/NMS spectrometer as shown in Fig. 1, we can evaluate the kinetic energy release (KER) values from the peak widths observed in PMS/NMS spectra. Hudgins et al. measured the maximum scattering angle corresponding to the highest fragment kinetic energy released for C_2H formation from $C_2H_2^+$ ions by using a neutral detection method [85]. The KER value was evaluated from full width at ten maximum (FWTM) of the peak associated with C_2H^- ions from $C_2H_2^+$ ions in PMS/NMS spectra [58]. This KER value at FWTM showed good agreement with maximum beam spread in the neutral detection method of Hudgins et al. de Bruijn and Los developed a position- and time-sensitive detector for the coincident measurement of two neutral fragments [33]. By using this method, they reported the precise kinetic energy distribution and dissociation mechanism of excited H_2 molecules formed from neutralization of H_2^+ with metal atoms containing alkali metals [34]. The KER values were evaluated from full width at half maximum (FWHM) of the peak associated with H^- ions formed from H_2^+ ions in the charge inversion mass spectrum with an alkali metal target [55]. The KER values of 8.2 eV in PMS/NMS spectra showed good agreement with kinetic energy distribution of 7–9 eV evaluated for H neutrals generated by the collision of H_2^+ ions with alkali metal targets by de Bruijn et al. [34].

3.2.2. Difference in dissociation mechanism between CID and PMS/NMS [65]

Fig. 4 shows the CID and charge inversion (PMS/NMS) mass spectra of CH_3OD^+ and CD_3OH^+. The target used for all these spectra was Cs, and the collision energy in the laboratory system was 3.0 keV.

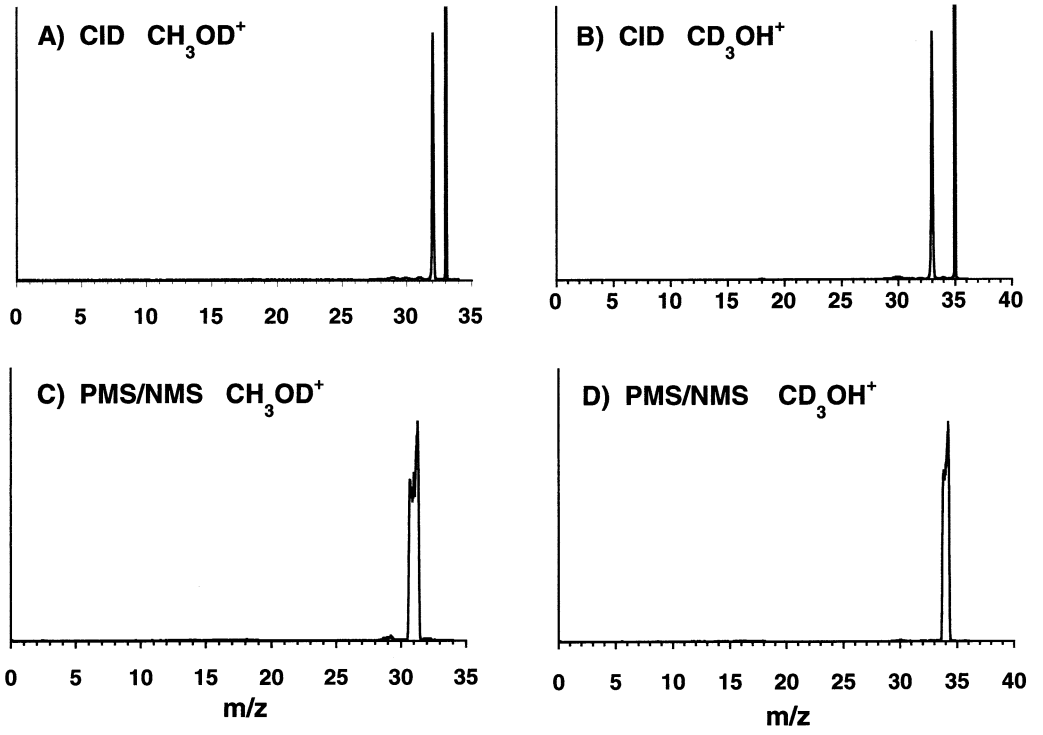

Fig. 4. CID spectra of (A) CH_3OD^+ and (B) CD_3OH^+; (C) the PMS/NMS spectra of CH_3OD^+, and (D) CD_3OH^+. The target was Cs. In both CID and PMS/NMS spectra, there is only one prominant peak associated with dissociative ions. Although the CID process involves the elimination of a hydrogen atom from the methyl group, the dissociative process in PMS/NMS results in the elimination of a hydrogen atom from the hydroxyl group.

Only one strong dissociative peak is observed in the CID spectra for both precursor ions. In the CID spectrum of CH_3OD^+ ($m/z = 33$) shown in Fig. 4(A), the mass number of the strongest peak is 32 which is attributed to the CH_2OD^+ ion resulting from elimination of a H atom from the methyl group. In the CID spectrum of CD_3OH^+ ($m/z = 35$) shown in Fig. 4(B), the dissociative species associated with the peak at $m/z = 33$ is attributed to the CD_2OH^+ ion resulting from elimination of a D atom from the methyl group. These results are consistent with the well known results for dissociation of methanol cation [86]. These results also indicate that scrambling of H atoms and D atoms does not occur in the precursor cations formed by electron impact ionization.

The predominant peak in the PMS/NMS spectrum of CH_3OD^+ ($m/z = 33$) [Fig. 4(C)] is the peak at $m/z = 31$, which represents a decrease in mass number of 2 from the parent ion. This reduction in mass number by 2 can be attributed to either the elimination of a D atom from the hydroxyl group or the elimination of two H atoms from the methyl group. Since in the CD_3OH^+ spectrum [Fig. 4(D)] the $CDOH^-$ ion having a mass number of 31 was not observed, the peak corresponding to mass number 31 is attributed to the CH_3O^- ion resulting from elimination of a D atom from the hydroxyl group. The predominant peak in the charge inversion spectrum of CD_3OH^+ ($m/z = 35$) [Fig. 4(D)] is the peak at $m/z = 33$, which is attributed to the CD_3O^- ion resulting from elimination of a H atom from the hydroxyl group. Therefore, the dissociation processes in both forms of partially deuterated methanol studied in this work appear to be the same. The elimination of a hydrogen atom from the hydroxyl group in PMS/NMS is in agreement with the major process in the

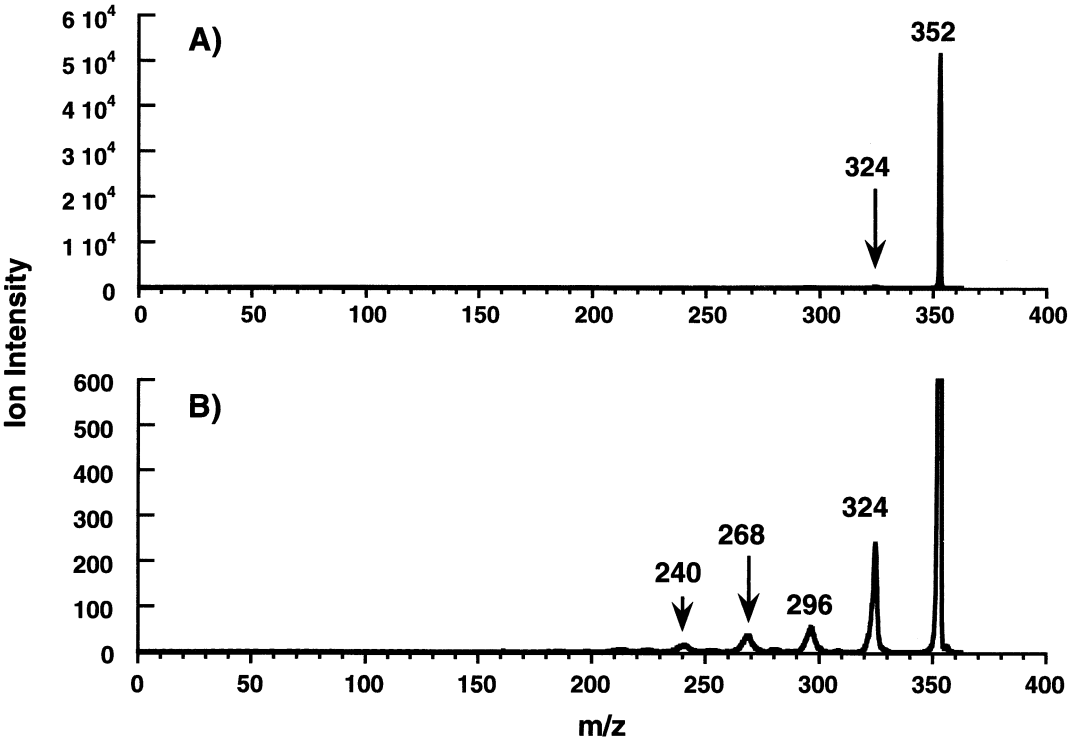

Fig. 5. CID spectrum of (A) $W(CO)_6^+$ ions and (B) with a magnified intensity scale. The $m/z = 184$ isotope of W was used for the precursor ions.

photoinduced dissociation of neutral methanol [87]. Because the activation energy of scrambling of hydrogen atoms is often higher in neutrals than in cations, this assignment, which neglects any scrambling, seems reasonable. These two charge inversion mass spectra show definitively that the dissociative process of the neutral species involves the elimination of a hydrogen atom from the hydroxyl group. These CID and PMS/NMS spectra clearly indicate different dissociation patterns for the cationic species and the neutral species. The agreement both of the neutral detection methods with the charge inversion mass spectrometry indicates most of the dissociation occurring in PMS/NMS takes place after exothermic neutralization of positive ions with alkali metal target [reaction (4)] and demonstrates that PMS/NMS is able to yield information about the dissociation of neutral species.

3.3. Internal energy distribution in PMS/NMS [64]

3.3.1. Difference in internal energy distribution between CID and PMS/NMS of $W(CO)_6$

The measured CID spectrum of $W(CO)_6^+$ ions is shown in Fig. 5. The target was Cs and the collision energy was 3.0 keV. The $m/z = 184$ isotope of W was selected for the precursor ions. The nondissociative $W(CO)_6^+$ peak at $m/z = 352$ is by far the strongest in the CID spectrum as shown in Fig. 5(A). The intensity of the $W(CO)_6^+$ peak is attributed mainly to precursor ions that did not interact with the target, whereas some of the $W(CO)_6^+$ ions may have been excited to energies below the dissociation energy of the W–CO bond. The main dissociative peaks at $m/z = 240$, 268, 296, and 324 observed in the magnified spectrum [Fig. 5(B)] are associated with $W(CO)_m^+$ ($m = 2$–5) ions resulting from cleavage of the W–CO bond. The

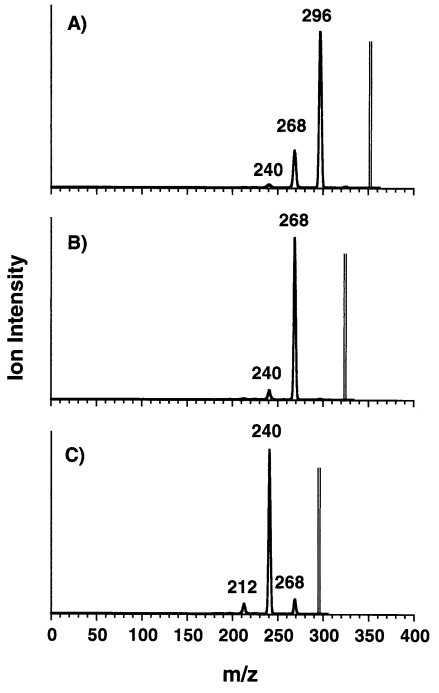

Fig. 6. PMS/NMS spectra of (A) $W(CO)_6^+$ ions, (B) $W(CO)_5^+$ ions, and (C) $W(CO)_4^+$ ions with a Cs target. Vertical double lines indicate the *m/z* values of the respective precursor ions. The experimental conditions of (A) were as same as those of Fig. 5 except for polarity of product ions. The peaks corresponding to the loss of two carbonyl ligands were by far the strongest apart from the peaks associated with the precursor ions.

larger the number of CO ligands lost, the lower the peak intensity becomes. Peaks associated with $WC(CO)_m^+$ ($m = 1–4$) resulting from CO triple bond cleavage in $W(CO)_m^+$ ($m = 2–5$) are also observed at *m/z* = 224, 252, 280, and 308, although the intensities of these ions are very weak. An internal energy of more than 10 eV is required for formation of $WC(CO)_m^+$ ions.

The PMS/NMS spectra of $W(CO)_n^+$ ($n = 4–6$) ions measured using a Cs target at the collision energy of 3.0 keV are shown in Fig. 6. Although the peak intensity of dissociative ions decreases with decreasing mass number in the CID spectrum shown in Fig. 5, the peak corresponding to the loss of two carbonyl ligands is the strongest in the PMS/NMS spectra for each of the precursor ions used. Even though the experimental conditions used to obtain the charge inversion spectrum are the same as those for the CID spectrum apart from the polarity of secondary ions, clear differences were found between the CID spectrum of Fig. 5(B) and the charge inversion spectrum of Fig. 6(A) of $W(CO)_6^+$ ions. Peaks associated with nondissociative negative ions corresponding to each of the $W(CO)_n^+$ ($n = 4–6$) precursor ions were not observed in any of the PMS/NMS spectra in Fig. 6. The very weak peak at *m/z* = 324 in Fig. 6(A) is attributed to $W(CO)_5^-$ ions. Because $W(CO)_5^-$ and $W(CO)_4^-$ ions are observed in Fig. 6(A), $W(CO)_5^-$ and $W(CO)_4^-$ ions are stable, and so the reason for the lack of peaks associated with nondissociative ions is not due to the instability of the corresponding negative ions. This result simultaneously provides evidence that dissociation after double electron transfer in a single collision is not the main process in PMS/NMS, as discussed in Sec. 3.1.

As shown in Fig. 6(C), the peak at *m/z* = 240 associated with $W(CO)_2^-$ resulting from the loss of two CO ligands from the parent ion is the dominant peak in the PMS/NMS spectrum of $W(CO)_4^+$, and is much stronger than the peaks associated with $W(CO)_3^-$ resulting from loss of one CO and $W(CO)^-$ resulting from loss of three CO molecules. Likewise, in the case of the spectra using $W(CO)_6^+$ and $W(CO)_5^+$ as the precursor ions, the peaks associated with $W(CO)_4^-$ and $W(CO)_3^-$ ions resulting from loss of two CO ligands from the parent ions were also dominant, as shown in Fig. 6(A) and (B), respectively. The dominant negative ion peak, therefore, appears to depend on the number of CO ligands lost from the precursor ion, rather than the number of CO ligands in the negative ion. The constancy of the number of CO ligands lost for the different parent ions suggests that the distribution of negative ions in the charge inversion spectra is determined not by the nature of the negative ions, such as their electron affinities, but rather by the internal energy of neutral species formed. Peaks associated with the nondissociative negative ion corresponding to each precursor ion were not observed, and peaks associated with $WC(CO)_m^-$ ($m = 0–5$) resulting from CO triple bond cleavage were also not observed in any of these spectra. This result indicates that the excitation was too low to

Table 3
Thermochemical data for $W(CO)_+^6$ and $W(CO)_6$; IE/AE are the ionization energies or appearance energies, and BE are bond energies; e_i and e_n are activation energies for fragmentation of ions and neutrals, respectively; IE/AE values are cited from Wysocki [18] BE(neutral–CO) values are cited from Venkataraman [88]

Ion	Ion			Neutral		
	IE/AE	e_i	BE(ion–CO)	Neutral	e_n	BE(neutral–CO)
$W(CO)_+^6$	8.5	0.0		$W(CO)_6$	0.0	
$W(CO)_+^5$	9.7	1.2	1.2	$W(CO)_5$	2.0	2.0
$W(CO)_+^4$	11.9	3.4	2.2	$W(CO)_4$	3.7	1.7
$W(CO)_+^3$	13.7	5.2	1.8	$W(CO)_3$	4.8	1.1
$W(CO)_+^2$	16.0	7.5	2.3	$W(CO)_2$	6.5	1.7
$W(CO)^+$	18.6	10.1	2.6	W(CO)	8.2	1.7
W^+	21.5	13.0	2.9	W	10.3	2.1

cause the dissociation of the CO triple bond, but was not sufficiently low for the precursors to survive. The level of excitation seems to have selected specifically for that required for cleavage of two W–CO bonds.

The thermochemical data for $W(CO)_6^+$ ions and $W(CO)_6$ neutral species are listed in Table 3. The data for $W(CO)_m^+$ ($m = 0-6$) ions were obtained from the measured ionization energy of $W(CO)_6^+$ ions and appearance energies of the fragment ions reported by Wysocki et al. [18]. The activation energies for fragmentation, e_{ion}, shown in Table 3 were obtained by subtracting the ionization energy from the appearance energy of each fragment ions. The corresponding bond energies were obtained by taking the difference between the consecutive activation energies e_{ion}. The data for $W(CO)_m$ ($m = 0-6$) were obtained from measured W–CO bond energies for $W(CO)_n$ reported by Venkataraman et al. [88] The activation energies for fragmentation, $e_{neutral}$, shown in Table 3 were calculated by summation of the corresponding bond energies.

Fig. 7(A) and (B) shows the internal energy distributions, $P(E)$, obtained for the PMS/NMS spectra and the CID spectrum, respectively, using the thermochemical data tabulated in Table 3. The internal energy distribution for the CID process was estimated from the measured peak abundances in our spectra shown in Fig. 5 using the same method as that reported by Wysocki et al. [18]. Our data and the results reported by Beranova et al. [89] use peak areas as peak abundance. The peak abundances in our data are based on peak areas for both CID and PMS/NMS spectra. The value at 0.6 eV which corresponds to the intensity of $W(CO)_6^+$ in the CID spectrum cannot be plotted because the intensity of the ions is attributed mainly to precursor ions. The plots in Fig. 7(B) are normalized at an internal energy value of 2.3 eV which corresponds to the intensity of $W(CO)_5^+$. The

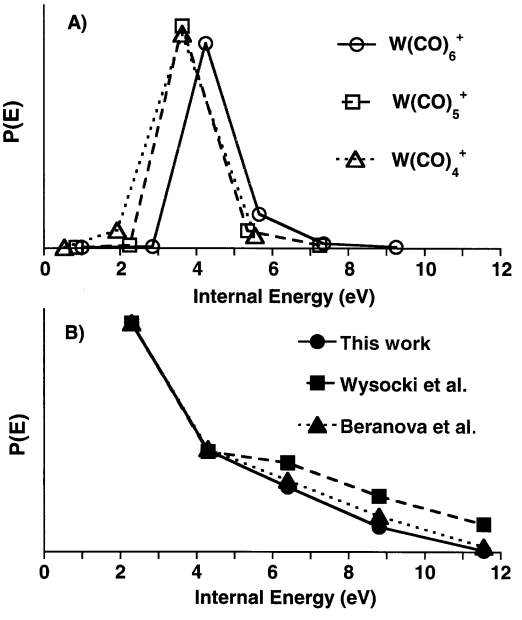

Fig. 7. Internal energy distributions, $P(E)$, (A) obtained for the PMS/NMS spectra shown in Fig. 6, and $P(E)$, (B) for the CID spectrum shown in Fig. 5, using the thermochemical data tabulated in Table 3. Precursor ions in (A) were $W(CO)_6^+$ (open circle); $W(CO)_5^+$ (open square); and $W(CO)_4^+$ (open triangle). Also shown in (B) are the $P(E)$ distributions for CID at 7 keV with an Ar target [18] and at 3 keV with an O_2 target [89].

features of the internal energy deposition for 3 keV collisions with a Cs target are similar to the high energy CID results using rare gas targets reported by Wysocki et al. [18] and an oxygen gas target reported by Beranova et al. [89]. This similarity is consistent with the empirical observation that quite different targets often function with similar effectiveness in terms of internal energy deposition in CID [16]. The P(E) intensities decrease with increasing internal energy, while there is a finite probability of depositing more than several electron volts of energy. Although the value at the lowest internal energy of 0.6 eV cannot be plotted, the internal energy distribution of the CID process is estimated to have a maximum at the lowest energy limit.

The internal energy distributions associated with the products in PMS/NMS were estimated from the known bond energy between W and CO ligands given in Table 3 and the measured peak abundance in the spectra shown in Fig. 6, in the same manner as for the estimation of internal energy distributions from CID spectra [18]. In contrast to CID, $P(E)$ distributions for PMS/NMS were narrow and were centered at similar values for each precursor ion. The excitation was not sufficiently high to cleave the CO bond, indicating that the excitation is less than 10 eV. Also, the lack of negative ions corresponding to precursor cations indicates that the excitation was not sufficiently low for the precursor cations to survive. The internal energy distribution function for the neutral products shows a maximum at 3–5 eV for all the precursor ions, as shown in Fig. 7(A).

The distributions plotted in Fig. 7(A) are the internal energy distributions of the excited neutrals from their respective ground states of $W(CO)_n$ ($n = 4-6$). As discussed in Sec. 3.1, the process of formation of the negative ions in PMS/NMS involves exothermic or thermoneutral neutralization, followed by spontaneous dissociation and then endothermic negative ion formation. The dissociation occurs from the neutral intermediates obtained by near-resonant neutralization. In order to clarify the reason for this energy distribution, the internal energy distribution as a function of the energy below the ionization levels are plotted in Fig. 8(A). The position of the peaks for all the precursor ions is approximately −4 eV. This value is in good agreement with the ionization potential of the Cs target of 3.89 eV.

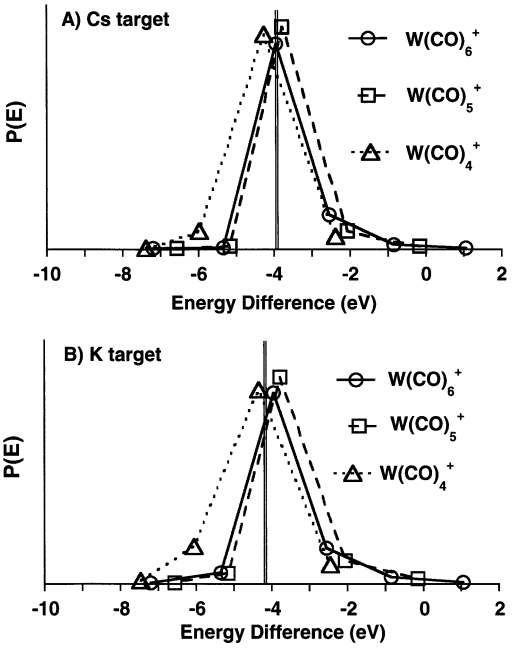

Fig. 8. $P(E)$ distribution plotted from the energy levels corresponding to the precursor ions for (A) a Cs target and (B) a K target. Precursor ions were $W(CO)_6^+$ (open circle); $W(CO)_5^+$ (open square); and $W(CO)_4^+$ (open triangle), respectively. Vertical double lines in the figures indicate the energy levels of resonant electron transfer process.

This correlation indicates that the neutralization reaction (3) is a near-resonant process. After near-resonant neutralization, the excited neutral dissociates spontaneously. The anionization process (5) is usually endothermic by 1–2 eV when alkali metal targets are used. If dissociation occurred in the anionization process, the internal energy distribution would be expected to disperse to the lower energy region as found for CID processes, which are endothermic. The sharp profiles of the internal energy distribution functions show that dissociation does not occur in the anionization process. These results are also accordance with the discussion in Sec. 3.1.

3.3.2. Absolute values for internal energy distribution in PMS/NMS

Heats of formation of $W(CO)_6$, $W(CO)_6^+$, and their fragments are shown in Fig. 9. Dissociation of thermometer molecules is proposed to require no activation energy, so the loss of two CO ligands from

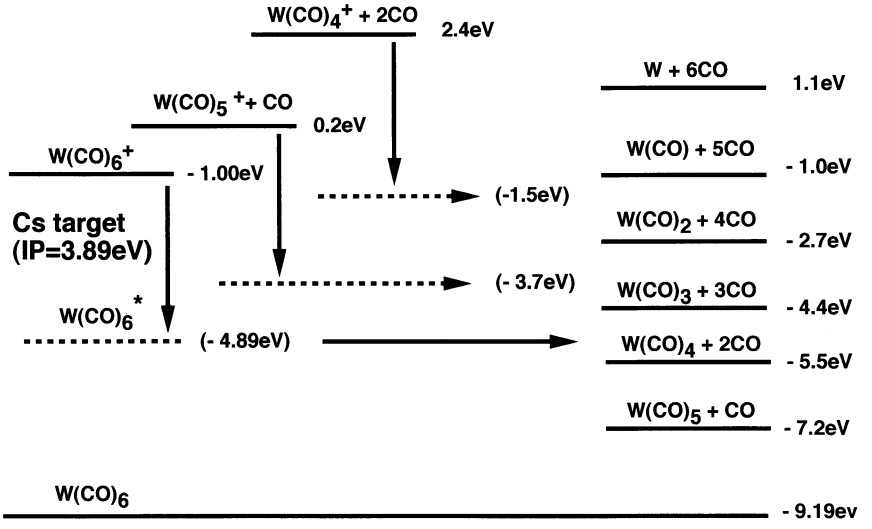

Fig. 9. Heats of formation of $W(CO)_6$, $W(CO)_6^+$ ions and their fragments in electron volts. The thermochemical data of $W(CO)_6$ and $W(CO)_6^+$ are from [70]. The data for fragments were taken from Table 3. The values shown in parentheses are the energy values predicted by near-resonant neutralization.

$W(CO)_6$ must be the result of formation of neutrals having energies between −4.4eV and −5.5 eV on the heat of formation scale shown in Fig. 9. Near-resonant neutralization of $W(CO)_6^+$ yields excited neutral intermediates which have an energy of 3.89 eV lower than the energy level of the corresponding cation. The near-resonant level for the resulting $W(CO)_6$ is −4.89 eV in the scale of heats of formation, which coincides with the region in which excited neutrals lose two CO ligands. The near-resonant levels for $W(CO)_5$ and $W(CO)_4$ also coincide with an internal energy which will result in loss of two CO ligands.

The internal energy distribution for the K target as a function of the energy below the ionization levels are also shown in Fig. 8(B). Although the internal energy giving the strongest peaks for the K target is the same as for Cs target, intensities in the lower internal energy is larger for the K target than the Cs target, for each of the precursor ions used. Because the near-resonant levels for the K target also coincide with an internal energy, which will result in loss of two CO ligands, the strongest peaks for the K target are the same as those for the Cs target. The difference in the internal energy distribution between the K target and the Cs target suggests that the energy level of the excited neutral is lower for the K target than the Cs target. Analysis of the internal energy distribution using the thermometer molecule $W(CO)_6$ demonstrates that neutralization in charge inversion mass spectrometry is a near-resonant process and that while the absolute value of internal energy can be estimated, it is not possible to distinguish clearly whether the differences in the energy levels of the excited neutrals is correlated with the ionization potential of the alkali metal target.

3.4 Dependence of dissociation mechanism on target species in PMS/NMS

3.4.1. Dependence of peak abundance and peak shape of dissociative negative ions on target species

Fig. 10(A), (B), and (C) shows the PMS/NMS spectra of acetylene cations using a Cs target, a K target, and a Na target, respectively. The peaks associated with C_2^- (m/z = 24) and C_2H^- (m/z = 25) resulting from loss of hydrogen atoms are predominant, whereas the peaks associated with CH_n^- (n = 0–2) (m/z = 12–14) resulting from the C–C triple

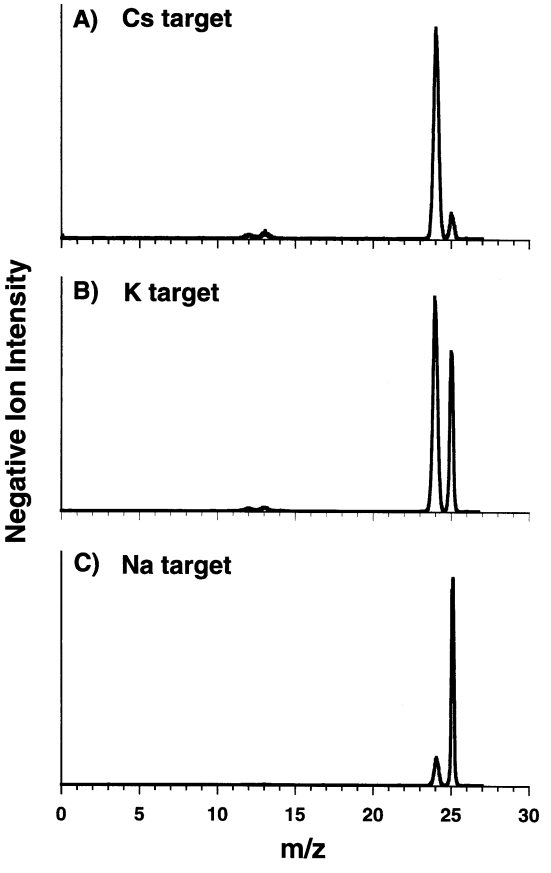

Fig. 10. PMS/NMS spectra of an acetylene cation using (A) a Cs target, (B) a K target, and (C) a Na target. The relative intensity of C_2^- ion peaks to C_2H^- ion peaks depend strongly on the target species.

bond cleaved are very weak. The relative ion intensity of $m/z = 24$ and 25 depends strongly on the target species, as seen in Fig.10. The relative intensity of C_2^- to C_2H^- evaluated from peak areas are 8.4, 1.6, and 0.21 for Cs, K, and Na target, respectively. Relative intensities of Cl^- to $C_6H_4Cl^-$ in PMS/NMS spectra of ortho-, meta-, and para-$C_6H_4Cl_2^+$ ions also depend on the target species [67]. In this case, the dependence of the relative intensities on the targets indicates clearly that the near-resonant states of the neutral intermediates in the PMS/NMS depend strongly on the target species, in contrast to $W(CO)_6$ where the dependence of the internal energy distribution on the target species was not obvious.

The CID spectra obtained using the Cs target and PMS/NMS using the Cs, K, and Na targets of CD_3OH^+ ion are shown magnified in Fig. 11. The dissociative peak observed in the CID spectrum at $m/z = 33$ in Fig. 11(A) is attributed to CD_2OH^+ ions. The peaks observed at $m/z = 34$ in the charge inversion spectra Fig. 11(B), (C), and (D) are attributed to CD_3O^- ions for each of the targets. The similarity of the peaks in Fig. 11(B), (C), and (D) indicates the dissociation patterns of the neutral species are independent of the type of target. The shape of the dissociative peaks in the CID spectrum in Fig. 11(A) resembles a triangle. This shape is typical of dissociative peaks observed in CID spectra generally, and is the result of dissociation from various internal energies [16]. The peak widths associated with CD_2OH^+ ions in the CID spectra were independent of the target species. This independence of target type is in accord with other work [2,16], which reports that different targets function with similar effectiveness in CID. Values for the kinetic energy release (KER) were calculated to be 0.04 eV using the FWHM of the CD_2OH^+ peak ($m/z = 33$). The small KER value of CID agrees with the internal energy distribution obtained using $W(CO)_6$ molecules, which has a maximum in the very low energy region as shown in Fig. 7(B).

On the other hand, the peak shape of the charge inversion mass spectra in Fig.11(B), (C), and (D) resembles a trapezoid. This shape suggests that dissociation is from a state with a specific internal energy [58,66]. Widths of the dissociative peak for the neutral species (CH_3OH^*) observed in the PMS/NMS spectra are much broader than those of the cations in the CID spectra. This difference suggests that the internal energy of the dissociative level in neutral dissociation is much higher than in ion dissociation. As seen in Fig. 11, the peak width of the charge inversion spectra become narrower as the ionization potential of the target increases. KER values for PMS/NMS spectra were calculated using the FWHM of the CD_3O^- peaks ($m/z = 34$), and these are listed in Table 4. The KER values become smaller as the ionization potential of the target increases. The dependence of the KER values on the target species

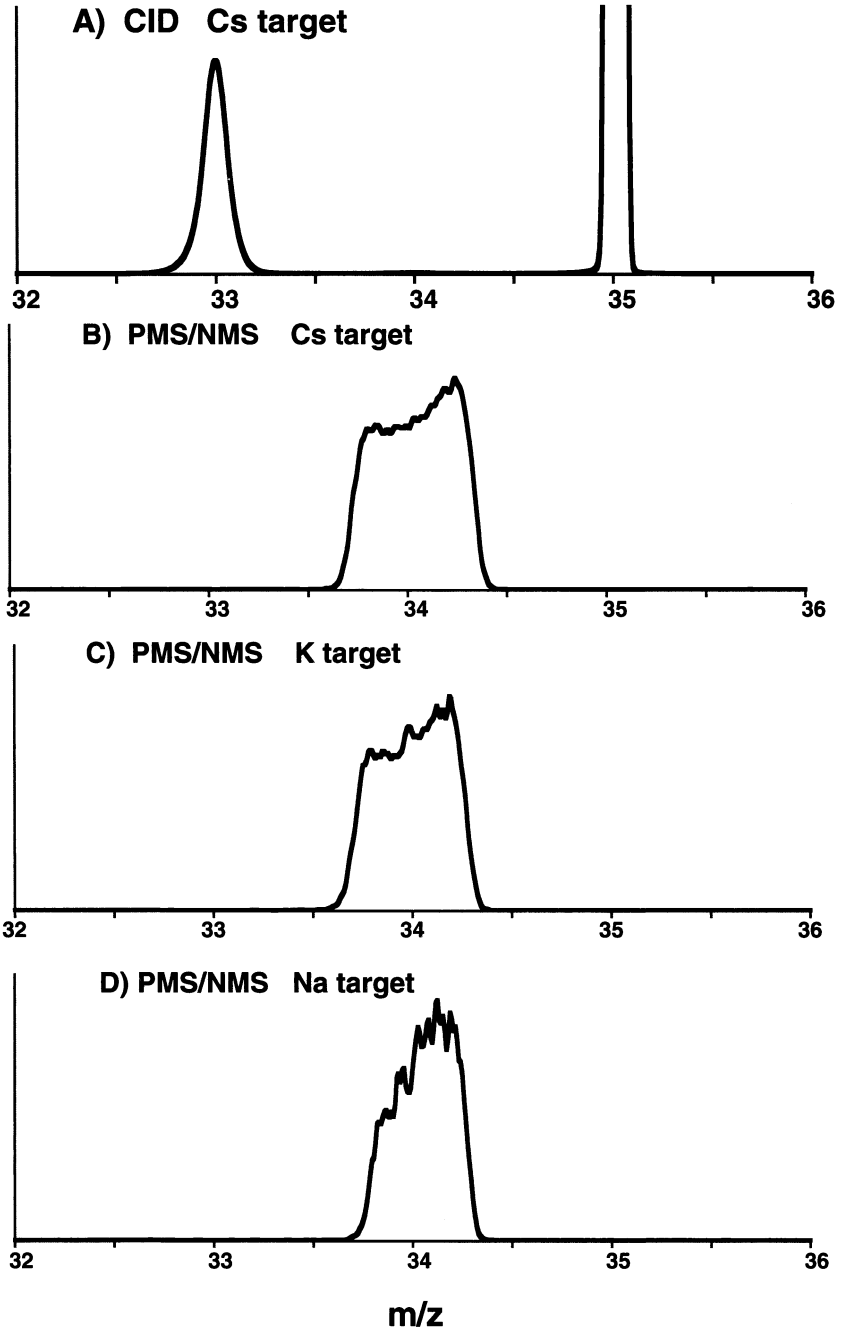

Fig. 11. Expanded CID spectrum of CD_3OH^+ using (A) a Cs target and (B) the expanded PMS/NMS spectra of CD_3OH^+ using a Cs target, (C) a K target, and (D) a Na target. The peak widths in the PMS/NMS spectra depend on the target species.

Table 4
Kinetic energy release (KER) values evaluated from the FWHM of the CD_3O ion peak observed in Fig. 11, ionization energies and available energies in electron volts, and ratios of the KER values to the available energy

	Cs target	K target	Na target	193.3 nm[a]
KER values	1.96	1.70	1.29	1.59 ± 0.13
Ionization energy	3.89	4.34	5.14	
Available energy	2.45	2.00	1.20	1.90
KER value / Available energy	0.80	0.85	1.07	0.82 ± 0.07

[a]See [87].

displays a trend similar to that of the relative intensity of C_2^- and C_2H^- peaks for the acetylene molecule (Fig. 10).

3.4.2. Dependence of internal energy distribution on target species in PMS/NMS [65]

Fig. 12 shows the heats of formation of the neutral species and the cations of CH_3OH and those of the fragments. In PMS/NMS, supposing that neutralization is resonant, as discussed from the results using $W(CO)_6$ molecules, the energy level of the formed neutral species should be lower than the level of the precursor cation by an amount equal to the ionization energy of the target. The energy levels associated with these resonance processes are also shown in Fig. 12. The available energies are the differences between these resonant levels of each target and the level of dissociative state CH_3O + H.

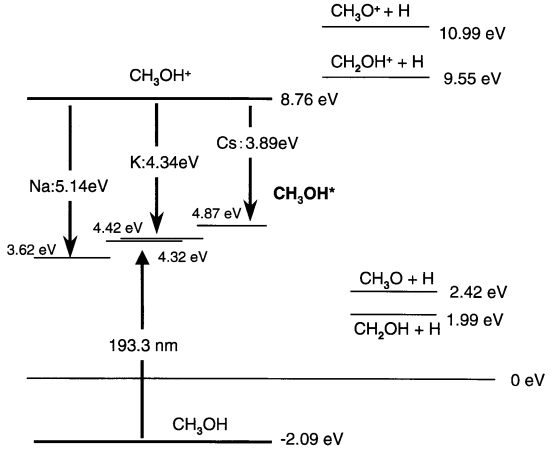

Fig. 12. Heats of formation of CH_3OH and CH_3OH^+ and their fragments in electron volts. Thermochemical values are taken from [70]. Also shown are the energy levels for near-resonant neutralization and for photoexcitation.

The major channel of dissociation induced by photoexcitation of CH_3OH at 193.3 and 157 nm has been reported to be direct hydroxyl H elimination; CH_3O + H [87,90,91]. The quantum yield of this process at 193.3 nm was determined to be 0.86±0.10 [87]. The excited CH_3OH produced by this photon was elucidated [87,90–92] as being in the 3s Rydberg state [93], which is purely repulsive in the O–H coordinate. The dissociation time from the Rydberg state is estimated to be shorter than 1 ps, since the dissociation is a direct process by way of the repulsive 3*s* surface [90–92]. The broad trapezoidal profile of the CH_3O^- peak in the PMS/NMS spectra is attributed to this direct dissociation [66]. The mean free time between neutralization and negative ion formation for the CH_3OH^+ ion is calculated to be about 100 ns from the ion velocity and the length of the target chamber. As the dissociation time is much shorter than the mean free time, dissociation of H atoms from excited CH_3OH molecules takes place before negative ion formation. The KER values and the ratios of the KER values to the available energies are compared with those in the photoexcitation experiment of Satyapal et al. [87] in Table 4. The available energy in the charge inversion spectra was estimated from the near-resonant state and the energy of the dissociative level, as seen in Fig.12. The available energy of K target was nearly equal to that for 193.3 nm photoexcitation. The close agreement of the KER values and the ratios with different excitation methods in Table 4 provides evidence that in charge inversion mass spectrometry, the neutralization is resonant, the excited neutrals dissociate to neutral fragments spontaneously, and the negative ions are formed from the neutral fragment by a second electron transfer. The smaller value of the ratio of the KER value to available energy for the Cs target in Table 4 is attributed to the excitation of CH_3O into a higher vibrational level. The larger value of this ratio for the Na target is attributed to the electron transfer to CH_3OH* having a higher energy level than resonance,

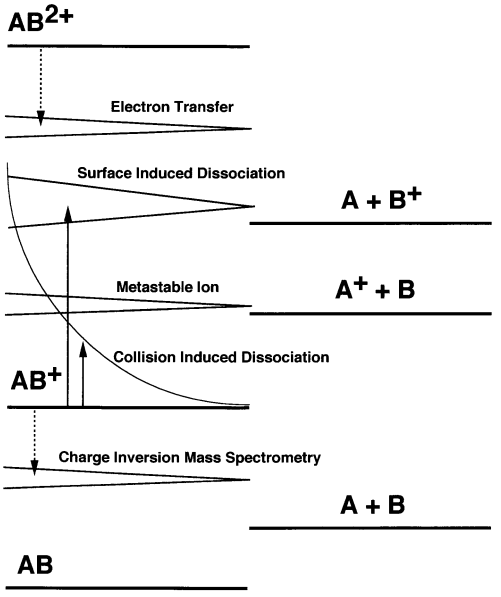

Fig. 13. Schematic representation of internal energy distributions in various types of tandem mass spectrometry. Activation and deactivation for the studied ions are indicated by solid and dotted line, respectively.

due to lack of the resonant state. The clear difference in the PMS/NMS spectra of both $C_2H_2^+$ and CD_3OH^+ using a Cs target compared with a K target indicates that the internal energy distribution in PMS/NMS is so narrow that the 0.5 eV difference in ionization potential between Cs and K becomes significant.

3.5. Dependence of internal energy distribution on activation method

Typical shapes of internal energy distribution and their relative position on the energy axis are illustrated in Fig.13 for isolated ions activated by different means. CID has a maximum at the low energy limit and has a long tail to higher energy beyond several electron volts, as shown in Fig. 7(B) [18–21]. The internal energy distribution of CID is wide, as shown schematically in Fig.13. For low-energy CID, the high energy tail is short, and the energy distribution can be controlled by changing the collision energy and the target density [18]. High-energy CID shows isomeric differentiation more clearly than low-energy CID owing to the high-energy tail, because direct dissociation becomes more dominant than the rearrangement process at high internal energy. For example, allene and propyne ions were differentiatied for ions in the mass range *m/z* 12–15 using high-energy CID [94,95]. However, the results in both of these reports are based on differences of only 1.5% of total ion abundance. This small difference is insufficient to prove that most of the isomeric $C_3H_4^+$ ions do not isomerize.

Metastable ions are situated only near the lowest dissociation limit. Since the energy distribution of metastable ions is very narrow, these ions showed isomeric differentiation for some molecules with rearrangement reaction. Surface induced dissociation can control the internal energy by changing the collision energy to the surface arbitrarily, and has a width of about a few electron volts [22–24]. Isomeric differentiation between allene ion and propyne ions was clearly achieved by controlling the collision energy with a fluorinated self-assembled monolayer (F-SAM) surface [15]. The internal energy distribution in electron transfer to doubly charged ions from a target yields a smaller width than SID [25–28], though ion intensities of doubly charged ions obtained by electron ionization are usually weak and the control of internal energy is achieved by changing the target species. To the best of our knowledge, isomeric differentiation between allene and propyne cannot be achieved by metastable ions or electron transfer to doubly charged ions. The isomeric differentiation observed in the SID spectra indicates that most of the stable $C_3H_4^+$ ions formed from allene and propyne by electron impact ionization do not isomerize. PNS/NMS gives clear differentiation between these isomeric $C_3H_4^+$ ions [61,62]. These results indicate that isomeric ions which are not differentiated by the conventional MS/MS technique are not always isomerized.

The differences between PMS/NMS and CID or SID indicate that the dissociation patterns of neutral species and cationic species are definitely different. It is expected that dissociation of neutral species will result in a higher probability of isomeric differentiation because the isomerization barrier for neutral species is higher than that of ions. The width of the

dissociative peak and its target dependence shows that the electronic state of excited neutrals can be selected using this technique. These results demonstrate that it is possible to study the dissociation of energy-selected neutrals by using the PMS/NMS techinique. Because ions of intermediates can be generated easily, PMS/NMS makes possible the study of the dissociation of unstable radicals obtained from the parent ions by way of near-resonant neutralization, such as vinylidene [63]. To give higher internal energy to the neutral intermediates in PMS/NMS, targets with smaller ionization energy, such as metastable neutrals, are required.

Acknowledgements

The author expresses his appreciation for the contributions of Dr. K. Arakawa and N. Morishita at JAERI, and to Mr. Tomozawa for help in collecting data.

References

[1] F.W. McLafferty, Tandem Mass Spectrometry, Wiley, New York, 1983.
[2] K.L. Busch, G.L. Glish, S.A. McLuckey, Mass Spectrometry/Mass Spectrometry: Technique and Applications of Tandem Mass Spectrometry, VCH, New York, 1988.
[3] R.G. Cooks, J.H. Beynon, R.M. Capriori, G.R. Lester, Metastable Ions, Elsevier, Amsterdam, 1973.
[4] T. Wachs, P.F. Bente, F.W. McLafferty, Int. J. Mass Spectrom. Ion Phys. 9 (1972) 333.
[5] F.W. McLafferty, P.F. Bente, R. Kornfeld, S.C. Tsai, I. Howe, J. Am. Chem. Soc. 95 (1973) 2120.
[6] F.W. McLafferty, R. Kornfeld, W.F. Haddon, K. Levsen, I. Sakai, P.F. Bente, S.C. Tsai, H.D.R. Schuddemage, J. Am. Chem. Soc. 95 (1973) 3886.
[7] J.H. Beynon, R.G. Cooks, J.W. Amy, W.E. Baitinger, T.Y. Ridley, Anal. Chem. 45 (1973) 1023A.
[8] R.A. Yost, C.G. Enke, J. Am. Chem. Soc. 100 (1978) 2274.
[9] R.A. Yost, C.G. Enke, D.C. McGilivery, D. Smith, J.D. Morrison, Int. J. Mass Spectrom. Ion Phys. 30 (1979) 127.
[10] R.A. Yost, C.G. Enke, Anal. Chem. 51 (1979) 1251A.
[11] M.A. Mabud, M.J. Dekrey, R.G. Cooks, Int. J. Mass Spectrom. Ion Processes 67 (1985) 285.
[12] M.J. Hayward, M.A. Mabud, R.G. Cooks, J. Am. Chem. Soc. 110 (1988) 1343.
[13] R.G. Cooks, T. Ast, M. A. Mabud, Int. J. Mass Spectrom. Ion Processes 100 (1990) 209.
[14] R.G. Cooks, T. Ast, T. Pradeep, Acc. Chem. Res. 27 (1994) 316.
[15] S. Hayakawa, B. Feng, R.G. Cooks, Int. J. Mass Spectrom. Ion Processes 167/168 (1997) 525.
[16] Collision Spectroscopy, R.G. Cooks (Ed.), Plenum, New York, 1978.
[17] K. Vekey, J. Mass Spectrom. 31 (1996) 445.
[18] V.H. Wysocki, H.I. Kenttämaa, R.G. Cooks, Int. J. Mass Spectrom. Ion Processes 75 (1987) 181.
[19] V.H. Wysocki, H.I. Kenttämaa, R.G. Cooks, J. Phys. Chem. 92 (1988) 6465.
[20] K.L. Schey, H.I. Kenttämaa, V.H. Wysocki, R.G. Cooks, Int. J. Mass Spectrom. Ion Processes 90 (1989) 71.
[21] S.R. Horning, M. Vincenti, R.G. Cooks, J. Am. Chem. Soc. 112 (1990) 119.
[22] M.R. Morris, D.E. Riederer Jr., B.E. Winger, R.G. Cooks, T. Ast, C.E.D. Chidsey, Int. J. Mass Spectrom. Ion Processes 122 (1992) 181.
[23] T. Ast, D.E. Riederer Jr., S.A. Miller, M.R. Morris, R.G. Cooks, Org. Mass Spectrom. 28 (1993) 1021.
[24] K. Vekey, A. Somogyi, V.H. Wysocki, J. Mass Spectrom. 30 (1995) 212.
[25] R.G. Cooks, T. Ast, B. Kralj, V. Kramer, D. Zigon, J. Am. Soc. Mass Spectrom. 1 (1990) 16.
[26] S.R. Horning, T. Kotiaho, L.E. Dejarme, J.M. Wood, R.G. Cooks, Int. J. Mass Spectrom. Ion Processes 110 (1991) 1.
[27] L.E. Dejarme, R.G. Cooks, T. Ast, Org. Mass Spectrom. 27 (1992) 667.
[28] R. Susic, L. Lu, D.E. Riederer Jr., D. Zigon, R.G. Cooks, T. Ast, Org. Mass Spectrom. 27 (1992) 769.
[29] G.I. Gellene, R.F. Porter. Acc. Chem. Res. 16 (1983) 200.
[30] P.M. Curtis, B.W. Williams, R.F. Porter, Chem. Phys. Lett. 65 (1979) 296.
[31] B.W. Williams, R.F. Poter, J. Chem. Phys. 73 (1980) 5598.
[32] G.I. Gellene, B.W. Williams, R.F. Porter, J. Chem. Phys. 74 (1981) 5636.
[33] D.P. de Bruijn, J. Los, Rev. Sci. Instrum. 53 (1982) 1020.
[34] D.P. de Bruijn, J. Neuteboom, V. Sidis, J. Los, Chem. Phys. 85 (1984) 215.
[35] D.P. de Bruijn, J. Neuteboom, J. Los, Chem. Phys. 85 (1984) 223.
[36] W.J. van der Zande, W. Koot, J. Los, J.R. Perterson, J. Chem. Phys. 89 (1988) 6758.
[37] S. Körnic, J.H.M. Beijersbergen, W.J. van der Zande, J. Los, Int. J. Mass Spectrom. Ion Processes 93 (1989) 49.
[38] J. Los, S. Körnic, J.H.M. Beijersbergen, J. Kistemaker, Int. J. Mass Spectrom. Ion Processes 93 (1989) 309.
[39] Y.K. Bae, M.J. Coggila, J.R. Peterson, Phys. Rev. Lett. 52 (1984) 747.
[40] J.R. Peterson, Y.K. Bae, Phys. Rev. A 30 (1984) 2807.
[41] Y.K. Bae, M.J. Coggila, J.R. Peterson, Phys. Rev. A 31 (1985) 3627.
[42] J.R. Peterson, Y.K. Bae, Phys. Rev. A 34 (1986) 3517.
[43] P. Devynck, W.G. Graham, J.R. Peterson, J. Chem. Phys. 91 (1989) 6880.
[44] J.R. Peterson, P. Devynck, C. Hertzler, W.G. Graham, J. Chem. Phys. 96 (1992) 8127.

[45] For reviews see: C. Wesdemiotis, F.W. McLafferty, Chem. Rev. 87 (1987) 485.
[46] For reviews see: J.L. Holmes, Mass Spectrom. Rev. 8 (1989) 513.
[47] F.W. McLafferty, Science 247 (1990) 925.
[48] For reviews see: N. Goldberg, H. Schuwarz, Acc. Chem. Res. 27 (1994) 347.
[49] For reviews see: D.V. Zagorevskii, J.L. Holmes, Mass Spectrom. Rev. 13 (1994) 133.
[50] F. Turecek, J. Mass Spectrom. 33 (1998) 779, and references cited therein.
[51] A.J. Frank, F. Turecek, J. Chem. Phys. A 103 (1999) 5348.
[52] M. Polasek, F. Turecek, J. Am. Chem. Soc. 122 (2000) 525, and references cited therein.
[53] For reviews see: C.A. Schalley, G. Hornung, D. Schroder, H. Schwarz, Chem. Soc. Rev. 27 (1998) 91.
[54] R. Srinivas, S. Vivekananda, S.J. Blanksby, D. Schroder, H. Schwarz, L.M. Fell, K. Terlouw, Int. J. Mass Spectrom. 197 (2000) 105, and references cited therein.
[55] S. Hayakawa, Int. J. Mass Spectrom. Ion Processes 90 (1989) 251.
[56] S. Hayakawa, K. Kadomura, K. Fujii, J. Mass Spectrom. Soc. Jpn. 43 (1995) 239.
[57] S. Hayakawa, N. Terazawa, N. Sugiura, J. Phys. B 23 (1990) 4539.
[58] S. Hayakawa, Int. J. Mass Spectrom. Ion Processes 116 (1992) 167.
[59] S. Hayakawa, A. Matsumoto, M. Yoshioka, T. Sugiura, Rev. Sci. Instrum. 63 (1992) 1956.
[60] S. Hayakawa, N. Terazawa, N. Sugiura, J. Mass Spectrom. Soc. Jpn. 41 (1993) 225.
[61] S. Hayakawa, H. Endoh, K. Arakawa, N. Morishita, T. Sugiura, Int. J. Mass Spectrom. Ion Processes 151 (1995) 89.
[62] S. Hayakawa, H. Endoh, K. Arakawa, N. Morishita, Int. J. Mass Spectrom. Ion Processes 171 (1997) 209.
[63] S. Hayakawa, M. Takahashi, K. Arakawa, N. Morishita, J. Chem. Phys. 110 (1999) 2745.
[64] S. Hayakawa, K. Harada, K. Arakawa, N. Morishita, J. Chem. Phys. 112 (2000) 8432.
[65] S. Hayakawa, K. Harada, N. Watanabe, K. Arakawa, N. Morishita, Int. J. Mass Spectrom. 202 (2000) A1.
[66] S. Hayakawa, M. Mori, N. Watanabe, F. Fujii, K. Arakawa, N. Morishita, J. Mass Spectrom. Soc. Jpn. 49 (2001) 144.
[67] S. Hayakawa, K. Taguchi, R. Kotani, K. Arakawa, N. Morishita, J. Mass Spectrom. Soc. Jpn., in press.
[68] B.L. Donnally, G. Thoeming, Phys. Rev. 159 (1967) 87.
[69] C.E. Moore, Atomic Energy Levels, Natl. Stand. Ref. Data Ser., Natl. Bur. Stand. 35 (1971).
[70] S.G. Lias, J.E. Bartmess, J.F. Liebman, J.L. Holmes, R.D. Levin, W.G. Mallard, J. Phys. Chem. Ref. Data 17 (Suppl. 1) (1988).
[71] R.D. Levin, S.G. Lias, Ionization Potentials and Appearance Potential Measurements 1971–1981, Natl. Stand. Ref. Data Ser., Natl. Bur. Stand. 71 (1982).
[72] K.M. Ervin, W.C. Lineberger, J. Phys. Chem. 95 (1991) 1167.
[73] W.J. Griffiths, D. Mathur, F.M. Harris, Int. J. Mass Spectrom. Ion Processes 87 (1989) R1.
[74] M.L. Langford, F.M. Harris, Rapid Commun. Mass Spectrom. 4 (1990) 125.
[75] W.J. Griffiths, M.L. Langford, F.M. Harris, Rapid Commun. Mass Spectrom. 10 (1996) 997.
[76] D. Mathur, Int. J. Mass Spectrom. Ion Processes 83 (1988) 203.
[77] D.P. Almeida, M.L. Langford, Int. J. Mass Spectrom. Ion Processes 101 (1990) 81.
[78] H. Tawara, A. Russek, Rev. Mod. Phys. 45 (1973) 178.
[79] Y. Nakai, T. Shirai, T. Tabata, R. Ito, At. Data Nucl. Data Tables 37 (1987) 69.
[80] D. Rapp, W.E. Francis, J. Chem. Phys. 37 (1962) 2631.
[81] J.B. Hasted, Physics of Atomic Collisions, Butterworths, London, 1964.
[82] T.J. Morgan, R.E. Olson, A.S. Schlachter, J.W. Gallagher, J. Phys. Chem. Ref. Data 14 (1985) 971.
[83] T. Tabata, R. Ito, Y. Nakai, T. Shirai, M. Sataka, T. Sugiura, Nucl. Instrum. Methods. Phys. Res. B 31 (1988) 375.
[84] J.B. Sedgwick, P.R. Nelson, C.A. Jordan, L.E. Abbey, Y. Xu, T.F. Moran, Chem. Phys. Lett. 146 (1988) 113.
[85] D.M. Hudgins, A.B. Raksit, R.F. Porter, Org. Mass Spectrom. 23 (1988) 375.
[86] N.L. Ma, B.J. Smith, J.A. Pople, L. Radom, J. Am. Chem. Soc. 113 (1991) 7903.
[87] S. Satyapal, J. Park, R. Bersohn, B. Katz, J. Chem. Phys. 91 (1989) 6873.
[88] B. Venkataraman, H. Hou, Z. Zhang, S. Chen, G. Bandukwalla, M. Vernon, J. Chem. Phys. 92 (1990) 5338.
[89] S. Beranova, C. Wesdemiotis, J. Am. Soc. Mass Spectrom. 5 (1994) 1093.
[90] Y. Wen, J. Segall, M. Dulligan, C. Wittig, J. Chem. Phys. 101 (1994) 5665.
[91] S. Harich, J.J. Lin, Y.T. Lee, X. Yang, J. Phys. Chem. A 103 (1999) 10324.
[92] C.C. Marston, K. Weide, R. Schinke, H.U. Suter, J. Chem. Phys. 98 (1993) 4718.
[93] J.B. Nee, M. Suto, L.C. Lee, Chem. Phys. 98 (1985) 147.
[94] W. Wanger, K. Levsen, C. Lifshitz, Org. Mass Spectrom. 15 (1980) 271.
[95] A.A. Mommers, P.C. Burgers, J.L. Holmes, J.K. Terlouw, Org. Mass Spectrom. 19 (1984) 7.